Food & Function

ROYAL SOCIETY OF CHEMISTRY

PAPER

View Article Online
View Journal

Cite this: DOI: 10.1039/d5fo04784f

Monitoring *in vitro* gastric bolus digestion with ultrasound

Xinhang Li, [a,b] Edoardo Capuano, [b] Chris L. de Korte [c] and Paul A. M. Smeets *[a]

Monitoring food degradation during gastric digestion is essential to understand how food properties impact nutrient absorption. Imaging techniques like ultrasound can be used to validate *in vitro* results *in vivo*. The aim was to assess the use of ultrasound (US) for monitoring changes in food bolus properties during *in vitro* gastric digestion with a newly designed model system. Artificial bread boli (n = 9) treated with amylase, pepsin or no enzyme underwent 90 minutes of static digestion (INFOGEST), during which US images were recorded. Bolus area and the number of pixels and Haralick image texture features were calculated. Average grey values were calculated at increasing distance from the bolus edge. The echogenic bolus area on ultrasound images increased over 90 min. From 10–60 min, amylase-treated boli were larger than pepsin-treated (ratios 2.00–2.40) and no enzyme boli (ratios 1.89–2.23). Regarding image texture, these boli had higher homogeneity and lower contrast than pepsin-treated boli. From 30 min onward, the bolus area of amylase-treated boli had 1.19–1.30 times higher homogeneity, and 2.5–4% lower *entropy*. From 10 min, the slope of the mean grey value curves for amylase-treated boli remained lower than for the other treatments. In the amylase-treated boli, an increase in homogeneity (rho = 0.8) and decreases in entropy (rho = −0.82) and slope (rho = −0.85) corresponded with increasing starch digestibility. These findings show the capacity of US imaging for quantifying bolus degradation *in vitro*. Future work should explore this novel application of US imaging in dynamic *in vitro* models and *in vivo*.

Received 5th November 2025,
Accepted 7th May 2026

DOI: 10.1039/d5fo04784f

rsc.li/food-function

1 Introduction

Food digestion is a complex combination of physiological, mechanical and biochemical processes that ultimately leads to the absorption of nutrients. These dynamic and individual-specific processes make experimental studies on human digestion particularly challenging. In addition, due to ethical, practical, and technical limitations, direct studies of *in vivo* human digestion can be difficult to conduct.[1]

Therefore, many *in vitro* digestion models have been developed, mimicking one or more digestion phases.[2] These can be classified as static or dynamic models, depending on their capacity to reproduce the dynamic physiological aspects of digestion (*e.g.*, gradual acidification or gastric emptying of the stomach). Static *in vitro* models, such as the INFOGEST method,[3] are widely used for assessing the digestibility of various food components. While they simplify digestive physiology and cannot mimic the complex dynamics of the digestive system, their straightforward design is effective for evaluating the impact of key factors such as pH and enzyme activity, making them quite suitable for mechanistic studies.[3,4] *In vitro* models provide controlled conditions and allow easy sampling. However, validating *in vitro* results against *in vivo* human digestion is challenging. Although the level of nutrient absorption can be analyzed by physiological indicators such as blood measurements, more direct and non-invasive techniques are needed to observe and characterize the preceding digestion mechanisms *in vivo*.

Validating *in vitro* findings *in vivo* may be achieved with imaging techniques such as magnetic resonance imaging (MRI), which can be used to connect *in vitro* and *in vivo* digestion models, because they can be used in both experimental settings.[5] Although MRI has emerged as a valuable tool in investigating gastrointestinal digestion, it is relatively expensive and requires participants to be positioned in the scanner tube, usually in a supine position. Another potential imaging technique is ultrasound (US) imaging. This technique is more affordable, widely available, and US machines are portable. US uses high-frequency acoustic beams to penetrate tissues, with reflections varying depending on acoustic impedance and reflector size, which is influenced by tissue properties such as

[a]*Division of Human Nutrition & Health, Wageningen University & Research, Stippeneng 4, 6708 WE Wageningen, The Netherlands. E-mail: paul.smeets@wur.nl*
[b]*Food Quality and Design Group, Wageningen University & Research, Wageningen, The Netherlands*
[c]*Medical Ultrasound Imaging Center, Department of Medical Imaging, Radboud University Medical Center, Nijmegen, The Netherlands*

density.[6] These reflections are captured by a transducer and converted into images, with the brightness of images increasing proportionally to the reflection strength. Ultrasound imaging is well-established for various clinical applications including preoperative assessment of the nature and volume of the gastric contents.[7] In research on gastric digestion, US has mainly been used to measure the rate of gastric emptying of different foods such as rye whole-meal bread and white wheat bread,[8] and viscous guar gum.[9] A study went beyond the assessment of gastric emptying and used US to monitor changes in the consistency of the gastric contents which differed in protein coagulation. For the same gastric antrum cross sectional area (CSA), calculated from the anteroposterior and craniocaudal diameters to represent gastric volume, lower plasma amino acid level was found for participants with curds compared with those without observed curds, suggesting that casein curd formation in the stomach leads to slower amino acid absorption, in addition to the apparent gastric volume changes.[10] This suggests that US could also be used to obtain quantitative measurements reflecting the properties and breakdown of ingested solid foods such as the particle size and texture. However, before such a novel approach could be applied *in vivo*, *in vitro* testing and validation is required to be able to establish US-based markers of digestion-related changes in food properties and their interpretation. A recent *in vitro* ultrasound study used through-transmission mode ultrasound with paired emitter and receiver to monitor gastric fluid migration and textural softening in potato and cheese slices during *in vitro* gastric digestion.[11] The effective diffusivity of the gastric fluid and the softening of solid food matrix were estimated from the variation of the ultrasonic velocity. Faster fluid migration and ultrasonic velocity increase were observed in potato than in cheese, consistent with the greater variation in hardness. While these findings indicate the potential of ultrasound for tracking digestive changes, this *in vitro* setup used a non-imaging approach rather than ultrasonographic imaging.

The aim of this study was to develop and test an ultrasound-based experimental setup for monitoring bread bolus breakdown during static *in vitro* gastric digestion, and to evaluate the extent to which ultrasound image information could be used to track digestion processes, including macrostructural breakdown of boli and changes in water content. To our knowledge, ultrasonography has not previously been used in tracking and visualizing the physical breakdown of food boli during *in vitro* gastric digestion. White bread was selected as a test product because it is widely consumed, and has a relatively uniform structure, which allows controlled and reproducible assessment of bolus breakdown.

2 Materials and methods

2.1 *In vitro* set-up development

We created a static *in vitro* digestion model – Gastric Ultrasound Model (GUSMO) tailored to allow US imaging of the gastric content (Fig. 1). It consists of a water bath (30 × 22 × 18 cm) and a repositionable frame that holds a polyethylene bag, simulating the stomach. The compartment can be heated and maintained at 37 °C with the use of a circulating heater and a cover. We ensured compatibility with both MRI and ultrasound scanning to allow comparison of both types of measurements. Accordingly, no magnetic materials were used and a rectangular "acoustic window" sealed with thin plastic film was incorporated, allowing a seamless interface between the ultrasound probe and the water in the bath. The US probe can be secured in a stable position with screws to ensure imaging with a consistent angle.

2.2 Preparation of bread boli

Commercial "Casino Wit Brood" was purchased from a local supermarket (Albert Heijn®, Netherlands). It refers to a Dutch white sandwich bread, typically baked in a rectangular loaf tin and pre-sliced, with a soft texture and relatively uniform crumb structure. The crust was removed after which slices of bread were cut into cubes of around 1 × 1 cm. Their thickness was the same as the original height of the toast, around 1.3–1.5 cm.

Fifteen grams of bread were moistened with 5 ml liquid including water, simulated saliva fluid (SSF) or gastric fluid (SGF). SSF and SGF were prepared according to the INFOGEST protocol.[3] Based on pilot trials, the INFOGEST 1 : 1 food-to-liquid ratio[3] produced excessively hydrated boli that collapsed too rapidly for ultrasound tracking. A lower ratio (15 g bread : 5 ml fluid) was therefore adopted to retain bolus integrity, in line with studies suggesting lower saliva incorporation during *in vivo* mastication.[12,13] To ensure effective contact between sample and enzymes in this static system with a large SGF volume and no gastric peristalsis, enzymes were incorporated into the boli during preparation rather than being added to the surrounding SGF. In addition, to distinguish the individual contributions of amylase and pepsin to structural changes, three different samples were produced where the 5 mL liquid was either: (1) 5 ml SSF with 0.1485 g amylase, (2) 5 ml SGF with 0.0125 g pepsin or (3) 5 ml Milli-Q water with no enzyme. The pepsin and amylase were diluted in simulated digestive fluid. α-Amylase from porcine pancreas (A3176, 10.1 activity units per mg) and pepsin from porcine gastric mucosa (P6887, 3200 activity units per mg) were purchased from Sigma-Aldrich (USA). The amylase and pepsin were applied at an activity of 75 U ml^{-1} and 2000 U ml^{-1} suggested by INFOGEST protocol. The total enzymatic activity was calculated based on the amount of bread sample and the 5 ml liquid used for bolus formation. Since enzymes were added during the bolus preparation step. Enzyme activities were converted to activity (U) per (g) nutrients. The final concentration of amylase and pepsin was approximately 196 U per g carbohydrate and 30 307 U per g of protein.

After mixing with one of the above solutions, samples were manually pressed and grinded 60 times using a mortar and pestle. Then the particles were collected and squeezed to form a ball, after which a board was used to press gently on each

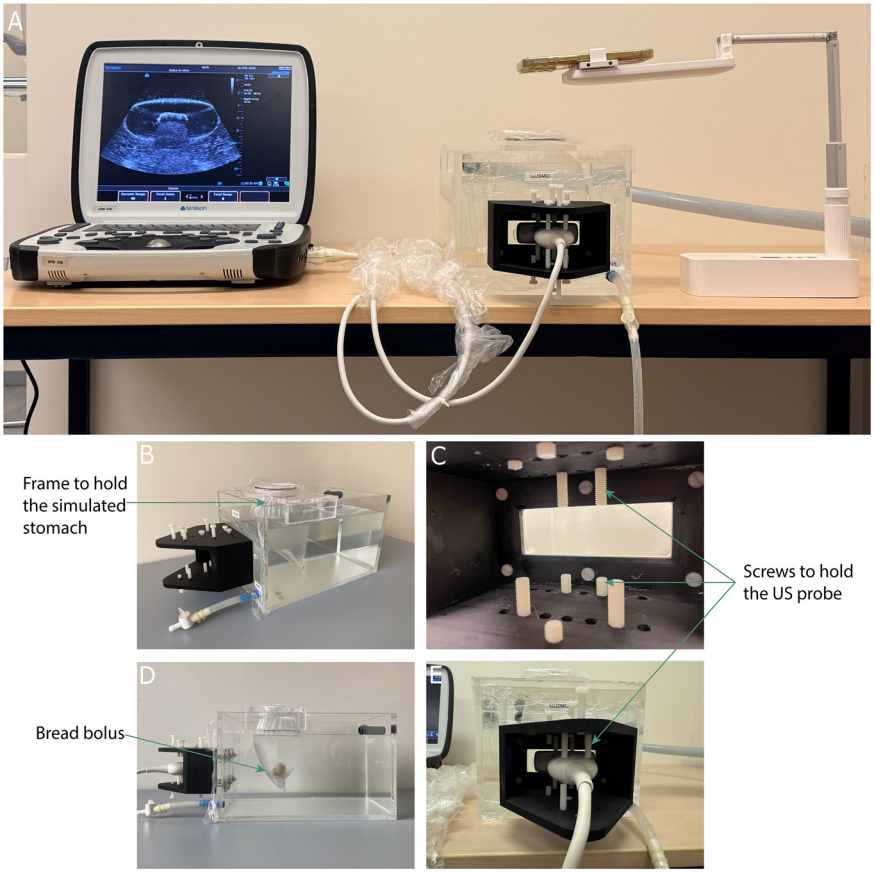

Fig. 1 *In vitro* setup of the Gastric Ultrasound Model (GUSMO). (A) An overview of the setup, including the ultrasound device (left), the GUSMO model (middle), and a phone holder (right) for recording top-view images of the bolus during digestion. (B) The water bath and the repositionable frame. (C) The "acoustic window". (D) The setup with a bread bolus in simulated stomach. (E) The US probe held by screws.

Fig. 2 Representative images of bread boli. (A) Bolus with amylase (196 units per g carbohydrate), (B) bolus with pepsin (30 307 units per g) and (C) bolus with no enzymes.

side to make the ball into a parallelepiped and make the surface as flat as possible. Several approaches were tested to shape the bolus, including the use of molds, syringes and mechanical compression using a texture analyzer. However, due to the high cohesiveness and adhesiveness of hydrated bread boli, these methods were not suitable, and manual shaping was adopted as a pragmatic approach. All bolus preparation steps were performed by a single operator, and bolus dimensions were controlled to remain within a comparable range (approximately 4–4.5 cm in length and 2–2.5 cm in width and height), to minimize size variability. Representative bread boli samples are shown in Fig. 2.

2.3 Physical property measurements

2.3.1 Moisture content measurement of boli. Before making them into the final shape ~0.5 g was taken of each bolus and dried in a hot-air oven at 105° for 24 hours. The difference in bolus weight before and after drying was used to calculate the initial (0 min) bolus moisture content percentage.

2.3.2 Density measurement. The weight of boli was measured with an analytical scale. To measure the volume, the drainage method was used: boli were placed in a measurement cylinder that contained a certain amount of water and then the water was pipetted out to arrive at the same volume. The weight of pipetted-out water was measured to determine the volume (1 g = 1 cm^3). The density of the bolus (g cm^{-3}) was calculated by dividing its weight (g) by the volume of water (cm^3).

To compare the changes in density and water content after digestion, boli with amylase were placed in 800 ml SGF and incubated for 10, 30, 60, and 90 minutes. After digestion, boli were picked from digestive fluid, and density and moisture measurements were taken as described above. For moisture measurement, the boli were dried in a hot-air oven until they were completely dry, instead of 24 hours. All measurements were done in triplicate.

2.4 Static *in vitro* gastric digestion

2.4.1 Simulated *in vitro* digestion. For the measurement of hydrolysis products, we separated the biochemical analysis from ultrasound scanning, considering the heterogeneous distribution of hydrolysates inside boli during static digestion. Boli were prepared in triplicate for each trial (with amylase or pepsin) and placed in beakers containing 800 ml SGF for 0, 10, 30, 60, and 90 min digestion, respectively. At the end of each trial, the boli were broken down in their surrounding fluid by using a food mixer for 30 s, and three 1 ml samples of the supernatant were collected. A workflow was shown as Fig. S1 in SI.

To stop the starch hydrolysis, absolute ethanol was added at a 1 : 4 ratio, mixed for 10 s and centrifuged at 10 000*g* for 10 min. For protein hydrolysis, the pH of sample was neutralized to around 7 by adding 1 M NaOH, followed by mixing for 10 s and centrifuging at 10 000*g* for 30 min. The centrifuged samples were stored in a freezer at −20 °C until further analysis.

2.4.1.1 Percent of digested starch. The supernatant taken from centrifuged samples was analyzed *via* measurement of the overall degree of hydrolysis quantified as glucose equivalent, using GOPOD format D-glucose Assay kits (Neogen, USA). To begin, 0.1 ml of supernatant was mixed with 0.5 ml amyloglucosidase solution in acetate buffer (0.1 M, pH 4.8) to convert all the products of amylase hydrolysis into glucose. The samples were then incubated at 37 °C for 1 hour to allow enzymatic hydrolysis, and heated to 100 °C for 10 min to inactivate enzyme.

After adding 3 ml of GOPOD reagent to 0.1 ml of sample solution, 200 μL of the mixture was sampled to a microplate. The percentage of digested starch was estimated by spectrophotometry (λ = 510 nm). The results were converted into starch equivalent concentrations using a conversion factor of ×0.9. The degree of starch hydrolysis at each time points was corrected using an initial blank prepared from blended no enzyme boli in SGF.

2.4.1.2 Degree of protein hydrolysis. The degree of protein hydrolysis was determined by measuring the concentration of released amino groups (–NH_2 groups) using the OPA (*o*-phthaldialdehyde) method. Serine standard solutions were used to generate a calibration curve for free amino acid groups. 15 mg 105.09 g mol^{-1} serine was diluted in 100 ml MilliQ water to prepare a L-serine stock solution. Eight serine solutions with concentrations of 0, 12.5, 25, 50, 75, 100, 150 and 200 mg L^{-1} were prepared by proportionally diluting the stock solution with water. The OPA solution was prepared just before measurement. 3.81 g sodium tetraborate was diluted in 80 ml MilliQ water. Once the sodium tetraborate was dissolved, 0.088 g dithiothreitol and 0.1 g sodium dodecyl sulphate were added. 0.08 g OPA was dissolved in 3 ml ethanol and was transferred to the 80 ml solution mentioned above after which MilliQ water was added to make a 100 ml solution. 24 μL of sample solution was mixed with 180 μL OPA reagents in microplates. The microplates were shaken in a microplate reader for 120 s and then read at λ = 340 nm to quantify the concentration of amino groups.

Bread samples of ~0.3 g were used for acid hydrolysis that was performed in triplicate. 2 ml of 6 M HCl was added to the bread in heating tubes. After heating at 110 °C for 24 h, the contents were neutralized with 1 M NaOH. 0.1 ml of the neutralized solution was diluted 50 times with Milli Q water. The concentration of amino acids was measured following the steps mentioned above. Degree of hydrolysis (DH) was expressed as the percentage of free amino groups released during digestion at 0, 10, 30, 60 and 90 min to the total amino groups released of complete hydrolysis, after correction by subtracting the initial blank, using the following formula:

$$\mathrm{DH}\,(\%) = \frac{[\text{Amino groups}]_{\text{digested}} - [\text{Amino groups}]_{\text{initial}}}{[\text{Amino groups}]_{\text{acid hydrolyzed}} - [\text{Amino groups}]_{\text{initial}}} \times 100$$

where $[\text{Amino groups}]_{\text{digested}}$ is the amount of free amino groups measured in the supernatant from blended pepsin-treated boli in SGF at a digestion time, $[\text{Amino groups}]_{\text{acid hydrolyzed}}$ is the amount after complete acid hydrolysis, and $[\text{Amino groups}]_{\text{initial}}$ represents the amount detected in the supernatant from blended no enzyme boli in SGF.

2.4.2 *In vitro* gastric digestion in the GUSMO. Boli were digested for 1.5 hours in 800 ml simulated gastric fluid. Reducing the volume was not feasible due to technical constraints related to the pressure of the surrounding water and imaging requirements. They were placed at the center of the bottom of the plastic bag. The initial pH of the SGF was adjusted to around 3.0 using 1 M HCL. With the circulating heater system, the temperature of the SGF was kept at 37 °C.

2.4.3 Ultrasound setting and measurements. US measurements were conducted with the use of a Terason uSmart 3300 ultrasound scanner (Terason@, USA) with a 5C2A curved linear array probe. The imaging settings used were as follows: scan depth, 15 cm; in-plane focus distance, 6 cm; dynamic range/contrast, 66 dB; frequency, 2.3 MHz; resolution, 0.0279 cm per pixel. Image Map F was used. The grey value distribution profile obtained from the image map reference bar

showed that the grey values within the relevant range represented in the acquired images were approximately linear. The gain and time gain compensation settings were kept constant throughout all imaging sessions.

US images of the gastric compartment were obtained at baseline (empty stomach compartment) and after placement of each bread bolus at 0, 5, 10, 15, 20, 25, 30, 35, 40, 45, 50, 55, 60, 75 and 90 min.

2.4.4 Image analysis. Boli were segmented by manually tracing their outer boundaries using wand tool, and the number of pixels was calculated (Fig. 3B) by the software QuPath 0.5.1 (University of Edinburgh, UK).[14] The segmentation was initiated from a seed point and expanded based on pixel intensity similarity and spatial continuity. The seed point was selected within visually representative regions of the bolus (typically relatively homogeneous and higher-intensity areas). In regions where the boundary between the hyperechoic bolus and the surrounding background showed a clear intensity transition, ROI delineation could be performed consistently. In lower contrast regions, where the bolus was not sufficiently distinct, the segmentation was adjusted using local intensity transitions and adjacent discontinuous hypoechoic background patches as cues to exclude background and image noise (examples are shown as Fig. S2 in SI). When the segmented regions approached the stomach wall (identified as a curved boundary), the brush tool was used to exclude areas within ~15 pixels of the wall to minimize artefacts caused by echo reflections at the plastic wall boundary. An example can

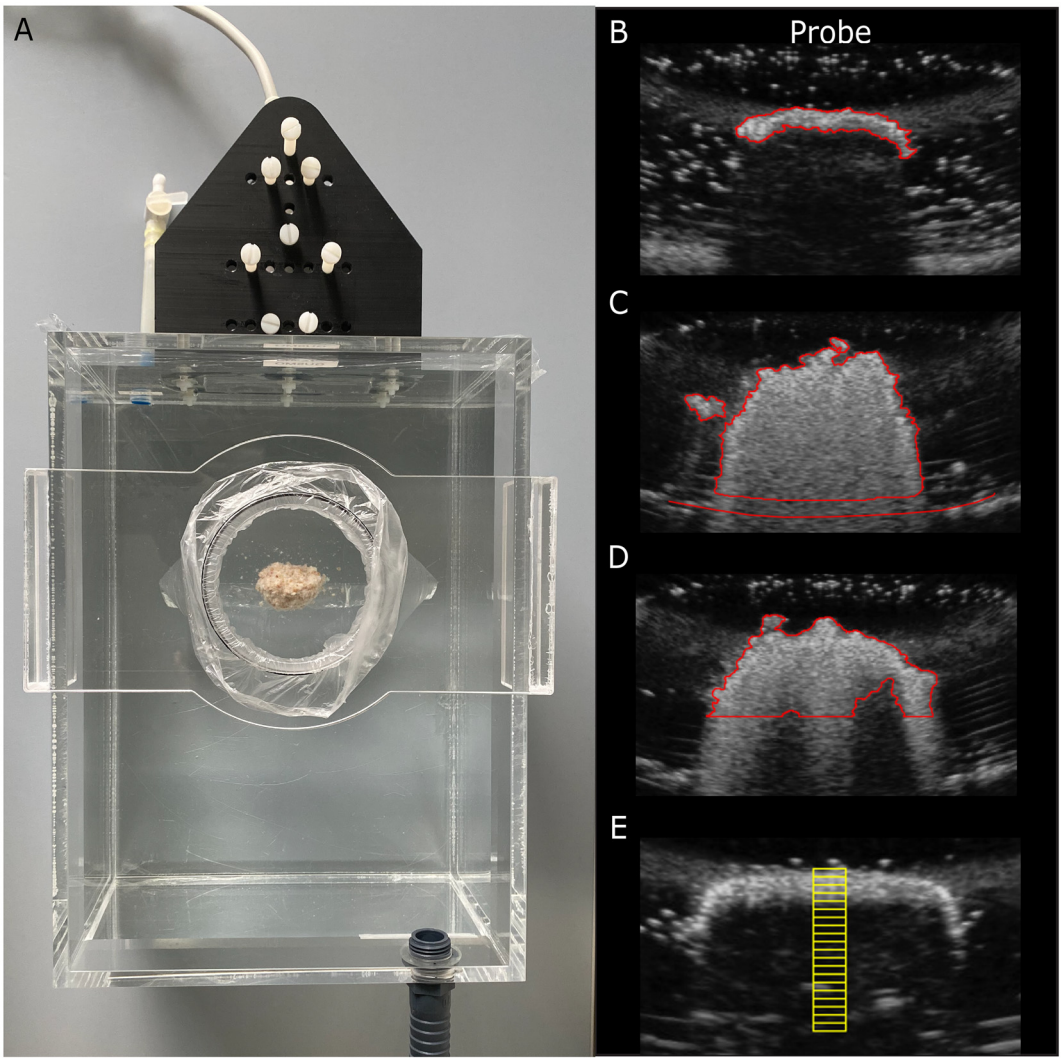

Fig. 3 Illustration of probe situation and ultrasound images. (A) Top view of a bolus in the gastric compartment. (B) Bolus segmentation. The position of the probe is the same as that shown in (A). The red trace indicates the outer area of the bolus. (C) Bolus segmentation and drawn stomach wall. The area between the lower edge of the segmented bolus and the stomach compartment wall (lower red line), within ~15 pixels of the wall (lower red line), was removed. (D) Constrained bolus area according to estimated bolus width during digestion. (E) The yellow rectangles on the image represent 20 regions of interest (ROIs), each containing 100 pixels. They are arranged at increasing depth from the edge of the bolus from closest to the probe to its core (farthest from the probe).

be found in Fig. 3C. In addition, a size constrained cut-off method based on estimated bolus size was used as a supplementary analysis. Bolus size at each digestion time point was estimated by scaling from its physical size at T_0, using the frame opening diameter (7 cm), and corresponding measurements from simultaneously captured top-view images. The estimated bolus width was then used as an upper boundary to constrain the segmented regions (Fig. 3D). Further details and results are provided in the SI (Fig. S3 and S4).

Five Haralick features including *Energy* (*Angular second moment*, *ASM; hereafter referred to as "homogeneity" in this study*), *Contrast*, *Correlation*, *Inverse Difference Moment* (*IDM*; *hereafter referred to as "local homogeneity"*), and *Entropy* were calculated for the bolus pixels based on Grey Level Co-occurrence Matrix (GLCM) which compares differences between neighboring pixels at 0°, 45°, 90° and 135° orientations.[15] These five features represent complementary aspects of image texture and constitute a widely adopted subset of the 14 Haralick features.[16–19] *Energy* (*Homogeneity*) measures the uniformity or orderliness of the texture. *IDM* (*local homogeneity*) measures the similarity of grey values. *Contrast* measures local fluctuations and variations among pixels. *Correlation* reflects the linear dependency of grey levels on those of its neighbors' intensity. *Entropy* represents the randomness and complexity of greyscale distribution.

20 regions of interest (ROIs), each containing 100 pixels (20 by 5 pixels), were manually placed at increasing distance from the edge of the bolus (Fig. 3E), gradually extending further away from the probe, which was locates at the top center of the ultrasound images. The mean grey value and standard deviation were calculated for each ROI using the software FIJI 2.16.0/1.54p (Fiji Is Just ImageJ, National Institutes of Health, US).[20] Subsequently, for each ultrasound image, the mean ROI grey value was plotted against the distance to the edge of the bolus. An example is shown in Fig. 4. To quantify the grey value trend, the slope of each line was calculated using the maximum point and the first point at which the mean grey value dropped below 100 (Fig. 4). The threshold of 100 was selected to minimize the influence of slight fluctuation of grey value in some images, especially in deeper ROIs, which may lead to inaccurate slope calculations.

2.5 Statistical analysis

All statistical analyses were performed in R 4.5.0. Normality of the data was assessed with quantile–quantile (Q–Q) plots of the residuals of dependent variables. The plots showed substantial deviations from normality, particularly with right tails, which violated the assumptions of linear models. Using a General Linear Mixed Model (GLMM) with a Gamma distribution and a log transformation of the dependent variables led to improvement in the distribution and outcomes. Model residuals were assessed using the DHARMa package to verify assumptions of homoscedasticity and model fit.

The model included main effects of enzyme treatments (amylase, pepsin, no enzyme), digestion timepoints (0, 10, 30, 60, 90 min), and treatments × time interactions, and sample as a random effect to account for repeated measures within samples. The dependent variations included slopes of mean grey value, size of bright areas and GLCM image features. This model was fitted using the glmmTMB package in R, and Type II Wald chi-square test was used to test the fixed effects using Anova function in car package. *P* values for the main effects and interactions were adjusted using Benjamini–Hochberg false discovery rate (FDR) correction used to control false positives. Statistical significance was set at $p < 0.05$. *Post hoc* pairwise comparisons were performed using estimated marginal means with Tukey test, and were only reported when the FDR-adjusted *p*-values of interactions indicated significance. All comparisons were based on differences between estimated marginal means, which represent the log-scale difference between conditions. Coefficients in log-scale were transformed to the original scale by taking the exponential of the estimates using the exp function. The back-transformed data were shown as estimated ratios with 95% confidence interval (CI) and *p* value (ratio, 95% CI, *p*). Estimated ratios represent the ratio of means between any two factor levels, such as the estimated ratio of mean homogeneity between amylase-treated and pepsin-treated boli. One-way ANOVA was used to analyze the changes in bolus moisture over time. Spearman correlation coefficients were calculated for digestibility of starch and protein, and the homogeneity, entropy and grey value curve slopes.

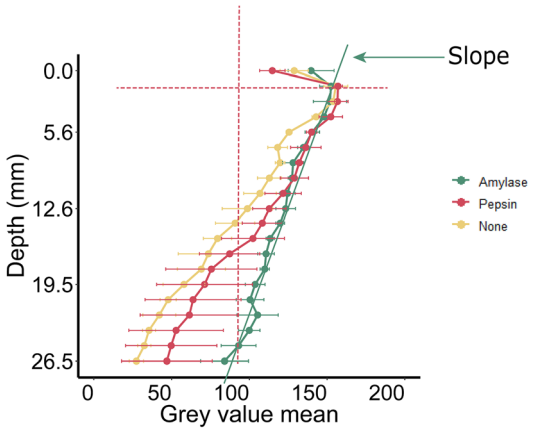

Fig. 4 Illustration of how the slope of the mean grey value curve was determined. The intersections of the red dashed lines with the grey value curve represent the peak point and the first point where the mean grey value dropped below 100. The slope of the green line connecting these points was calculated.

3 Results and discussion

3.1 Monitoring structural breakdown by ultrasound images

3.1.1 Bolus size. Fig. 5 shows examples of segmented bolus areas (top panel) and the results of the bolus area and image texture feature analysis. Consistent with changes visible in the ultrasound images, there was a strong main effect of time on the size of boli ($\chi^2 = 845$, $p_{FDR} < 0.0001$). The bolus area

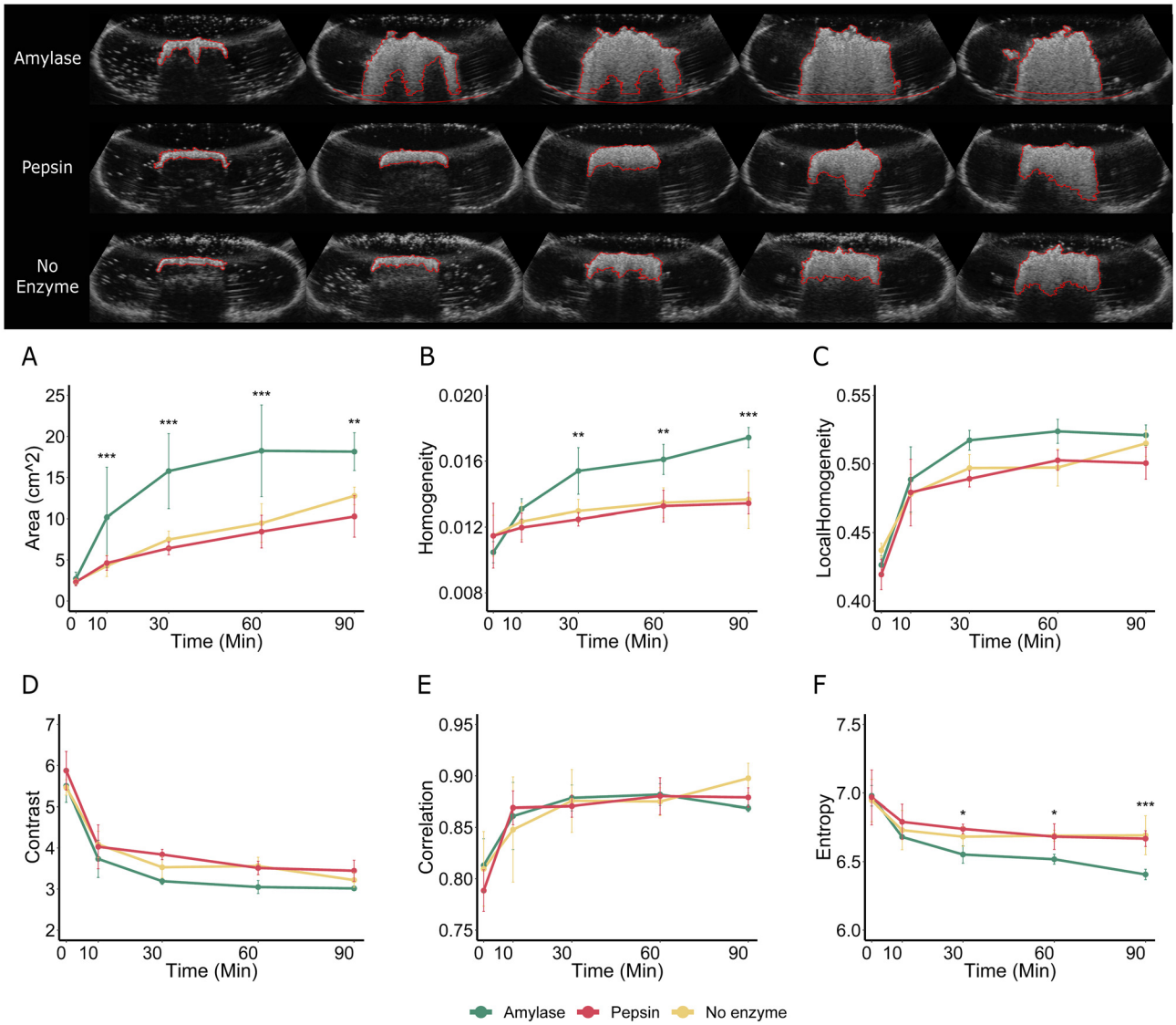

Fig. 5 Representative images of bolus inserted in amylase (top row), pepsin (middle row) and no enzyme (bottom row) with segmentation and results (A–F) of GLCM texture analysis for the traced regions over the 90-minute digestion. (A) size of segmented bolus ROIs; (B) homogeneity measures the uniformity or orderliness of the texture. Higher values indicate less texture complexity; (C) local homogeneity represents similarity of grey values. Higher values indicate a smoother image/area; (D) contrast reflects differences in greyscale intensities. Higher contrast values indicate greater differences; (E) correlation reflects the degree to which a pixel's intensity is linearly related to its neighbor's intensity; (F) entropy represents the randomness and complexity of greyscale distribution; higher entropy values indicate more complex and disordered texture. Asterisks (*) indicate significant differences for amylase-treated boli compared to pepsin-treated and no enzyme boli. *p < 0.05, **p < 0.01, ***p < 0.001. For bolus area at t = 90 and entropy at t = 30, the significance refers only to amylase *versus* pepsin.

increased progressively from 0 to 90 minutes across all experiments. This reflects swelling of the boli during digestion. The main effect of enzyme treatment (χ^2 = 22.6, p_{FDR} < 0.0001) and the interaction of time and treatment were found (χ^2 = 36.3, p_{FDR} < 0.0001). Comparison of the enzyme treatments at each time point showed that as expected there was no difference in bolus size between the treatments at 0 min. From t = 10 to t = 60 min, the bolus size of amylase-treated boli was larger than that of pepsin-treated boli and of boli with no enzyme (p < 0.001) (Table 1). At t = 90 min, it was larger than pepsin-treated boli (p < 0.01) but not significantly different from that of no enzyme boli (p = 0.1). The largest difference was found at 30 min, when the size of amylase-treated boli was on average 2.40 times (p < 0.0001) larger than that of pepsin-treated boli. For the comparison between amylase and no enzyme treatments, the greatest difference was found at 10 min, with the amylase-treated boli being on average 2.23 (p < 0.0001) times larger than the no enzyme boli. There were no differences between the pepsin-treated and the control boli at any time point (all $p \geq 0.38$).

These results indicate that ultrasonography can be used to track changes in the swelling of boli during *in vitro* gastric

Table 1 Pairwise comparisons for the treatments × time interaction on bolus size

Treatment comparison	Time (min)	Ratio[a]	95% CI	*p*
Amylase/no enzyme	0	1.11	0.74, 1.67	0.81
	10	2.23	1.49, 3.35	<0.0001
	30	2.07	1.38, 3.10	0.0001
	60	1.89	1.26, 2.83	0.0007
	90	1.42	0.95, 2.13	0.1
Amylase/pepsin	0	1.15	0.77, 1.73	0.69
	10	2.00	1.33, 3.00	0.0002
	30	2.40	1.60, 3.60	<0.0001
	60	2.12	1.42, 3.18	<0.0001
	90	1.79	1.19, 2.68	0.002

[a] Estimated ratio of marginal mean bolus size for amylase-treated boli to that of no enzyme boli or the pepsin-treated boli. Ratio and 95% CI are back-transformed from GLMM contrasts on the log scale.

Table 2 Pairwise comparisons for the treatments × time interaction on homogeneity

Treatment comparison	Time (min)	Ratio[a]	95% CI	*p*
Amylase/no enzyme	0	0.92	0.80, 1.04	0.26
	10	1.06	0.93, 1.21	0.53
	30	1.19	1.04, 1.36	0.0068
	60	1.20	1.05, 1.37	0.0044
	90	1.28	1.12, 1.46	<0.0001
Amylase/pepsin	0	0.92	0.80, 1.05	0.27
	10	1.10	0.96, 1.25	0.24
	30	1.24	1.08, 1.41	0.0006
	60	1.21	1.06, 1.39	0.0018
	90	1.30	1.14, 1.48	<0.0001

[a] Estimated ratio of marginal mean homogeneity for amylase-treated boli to that of no enzyme boli or the pepsin-treated boli. Ratio and 95% CI are back-transformed from GLMM contrasts on the log scale.

digestion. The addition of amylase promoted bolus expansion and degradation, while pepsin-treated boli hardly differed from the control boli with no enzyme added. As digestion progressed, we observed an increase in the bolus area over time. The expansion during digestion is consistent with matrix weakening caused by hydrolytic process, which improves water penetration and structural softening, as previously reported in gastric digestion studies.[21] When hydrolytic effects on the matrix components are limited, structural changes and associated swelling are correspondingly weakened. This interpretation is supported by previous finding showing limited proteolysis of bread proteins during gastric digestion.[22]

In the present study, the boli may undergo a transition from a heterogeneous structure, consisting of fine bread chyme, porous bread crumbs and entrapped gas pockets. As digestion progresses, fluid infiltration may reduce these structural differences, resulting in a more uniform structure with a more homogeneous density distribution. In addition, the small air pockets within the boli induce scattering and attenuation of sound waves. This is because the small air inclusions have a high attenuation coefficient, preventing further penetration of the ultrasound in the bolus. This is clearly illustrated at $t = 0$, where the heterogeneous structure of bolus and small air pockets lead to strongly reduced penetration and result in only tiny bright areas. From 10 to 90 min, as gastric fluid infiltrates the boli, these air pockets will be dissolved and replaced by water, which would cause a decrease in attenuation and a gradual increase in penetration. This would result a larger bolus area in the ultrasound images. Consequently, we used image texture features, which have been shown to be useful to characterize material properties.[23,24]

3.1.2 Image texture: Haralick features. Among all the 5 Haralick features, *homogeneity* and *entropy* showed the largest difference across groups. For *homogeneity*, the GLMM results showed main effects of enzyme treatment ($\chi^2 = 19.4$, $p_{FDR} = 0.0001$) and digestion time ($\chi^2 = 116$, $p_{FDR} < 0.0001$), as well as an interaction of treatment and time ($\chi^2 = 36.4$, $p_{FDR} < 0.0001$). From 30 to 90 min, the bolus areas of amylase-treated boli had higher *homogeneity* than control boli and pepsin-treated boli (Table 2). The largest difference in *homogeneity* was observed at 90 min, and the *homogeneity* of amylase-treated boli was on average 1.30 and 1.28 times higher than that of pepsin-treated boli and no enzyme boli ($p < 0.0001$ and $p < 0.0001$, respectively). No difference was found between no enzyme boli and those with pepsin (all $p \geq 0.77$).

Similarly, the GLMM results showed main effects of enzyme treatment ($\chi^2 = 16.0$, $p_{FDR} = 0.0004$) and digestion time ($\chi^2 = 146$, $p_{FDR} < 0.0001$), as well as an interaction of treatment and time ($\chi^2 = 20.5$, $p_{FDR} = 0.017$) for the *entropy* of the bolus areas. *Entropy* in amylase-treated was 97% of that in pepsin-treated and no enzyme boli at $t = 60$ min ($p = 0.031$ and $p = 0.023$). At $t = 90$ min, *entropy* of amylase-treated boli was approximately 4% lower than that of pepsin-treated and no enzyme boli ($p = 0.0001$ and $p < 0.0001$). In contrast, there were no differences between the pepsin and no-enzyme boli (all $p \geq 0.64$).

For *local homogeneity* and *contrast*, a main effect of treatment was observed with the bolus areas of amylase-treated boli having a higher *local homogeneity* ($\chi^2 = 17.8$, $p_{FDR} = 0.0002$) and lower contrast ($\chi^2 = 23.4$, $p_{FDR} < 0.0001$), than no enzyme and pepsin-treated boli. For *correlation*, there was no main effect of treatment, but an effect of time ($\chi^2 = 143$, $p_{FDR} < 0.0001$). No treatment × time interaction was found in *local homogeneity*, *contrast* and *correlation* (*local homogeneity*, $p = 0.09$, contrast, $p = 0.22$, correlation, $p = 0.21$). Overall, these results demonstrate that digestion progression was reflected in all 5 Haralick features. Amylase, but not pepsin induced increased bolus *homogeneity*, and reduced *entropy* on ultrasound images which likely reflects bolus degradation. This is consistent with previous studies on starch-rich food digestion, where starch hydrolysis has been shown to contribute to food matrix breakdown and a softer structure.[25] Such structural breakdown and mixing processes are known to lead to a more homogeneous digesta. In contrast, limited proteolysis in gastric phase may provide context for the relatively minor changes at macroscopic level observed in starch-rich bread.[26]

As *homogeneity* indicates the uniformity and smoothness within an image, and *entropy* measures the disorder, randomness and complexity of pixels, these results suggest that the

image texture is more uniform due to enzymatic breakdown and fluid infiltration. Moreover, as shown in Fig. 5, the trends of *contrast*, which captures the variations in intensity between a reference pixel and its neighbors, were opposite to those of *homogeneity* and *correlation*. Ultrasonography with GLCM analysis has widely been used in clinical diagnosis. For example, a study developing a non-invasive, automatic approach for diagnosing abdominal malignant tumors, including the hepatocellular carcinoma and the colorectal tumors, found that GLCM *homogeneity* and *contrast* characterized the heterogeneity of tumoral tissue arising from the coexistence of regions with necrosis, fibrosis, and active growths.[27] Quantitative image analysis showed that normal livers have higher *homogeneity* and lower *contrast* than fibrotic livers, reflecting well-organized tissue architecture of healthy liver tissue and the structural disorganization associated with fibrosis.[28] This results was also consistent with an MRI study, which found that *entropy* and *contrast* were good discriminative features for identifying fibrosis.[29] MRI studies on coagulation during gastric digestion found that lower *homogeneity* and higher *contrast* could indicate a higher degree of coagulum formation, and higher *homogeneity* may reflect not only a more homogenous liquid, but also the presence of a large and fairly homogenous coagulum.[24,30] These findings suggest that the increase in *homogeneity* and *correlation*, along with decrease *contrast* and *entropy* in our study may be attributed to reduced heterogeneity of bolus during digestion.

3.1.3 Bolus grey value analysis. Fig. 6 shows representative bolus pictures and corresponding ultrasound images that show swelling and breakdown of the samples over the 90-minute simulated gastric digestion. In all treatments, the high-echogenicity (bright) regions gradually expand, regardless of enzyme addition. At time 0 the bright areas on the ultrasound images are consistently small for all treatments, indicating that soundwaves have only limited penetration probably caused by the presence of small air bubbles leading to severe attenuation of the ultrasound signal. However, from 10 minutes onwards, significant expansion of the bright bolus areas can be observed in amylase-treated boli (Fig. 6, top panel) compared with the other two treatments (middle and bottom panels). These changes are consistent with what can be seen in the photographs. Amylase-treated boli appeared more swollen with visible fragmentation at the periphery, while for boli with pepsin and no enzyme, minimal changes

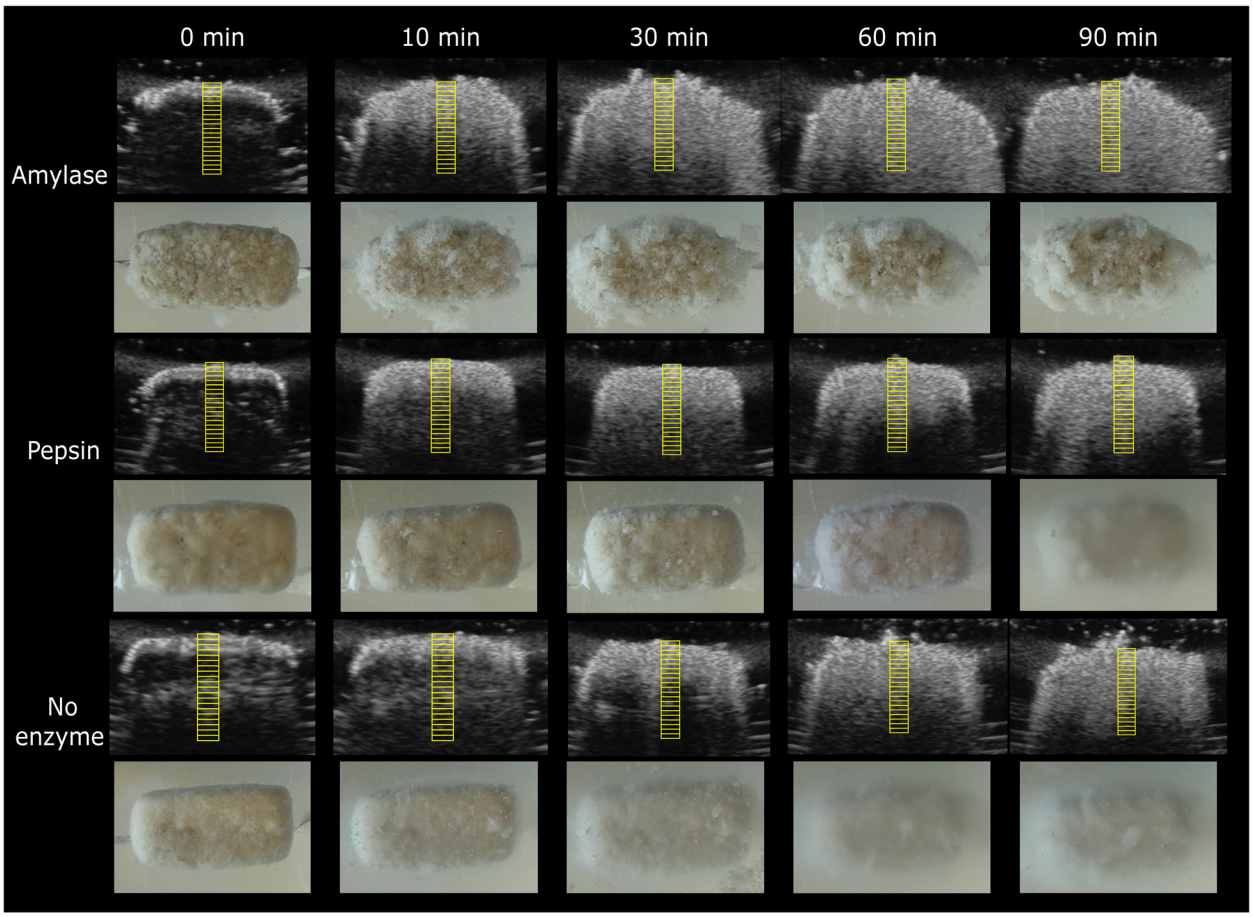

Fig. 6 Representative ultrasound images and pictures of bread boli taken at different digestion time points. The panels, from top to bottom, show images of bread boli containing amylase, pepsin or no enzyme (control). The yellow rectangles represent 20 manually positioned adjacent regions of interest (ROIs, 20 × 5 pixels). These ROIs are vertically aligned along the middle of the bolus, beginning at the edge of bolus.

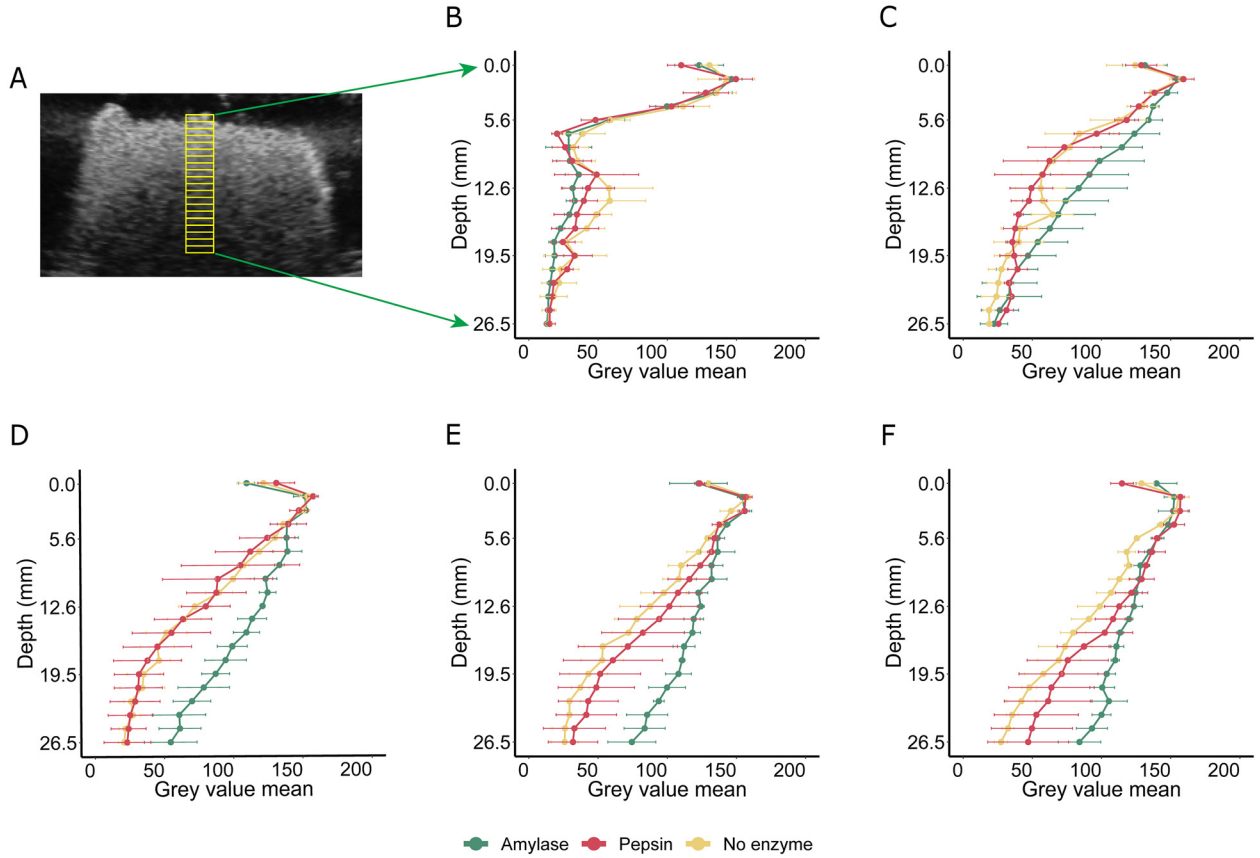

Fig. 7 Mean ± SD grey value of ROIs over 90 minutes digestion. (A) Example of a bolus ultrasound image with 20 adjacent ROIs. The first ROI at the edge of bolus is defined as 0 mm in the graphs, and last one is located at ~26 mm depth. Panels (B)–(F) show the mean grey value of the ROIs at 0, 10, 30, 60 and 90 min, respectively, comparing among boli with amylase, pepsin and no enzymes. All measurements were done in triplicate.

are visible over time. Overall, these ultrasound images show that ultrasonography can be used to track macrostructural changes in food boli during gastric digestion.

To quantify the changes over time and differences between the treatments grey value changes across the bolus were examined (Fig. 7A). The GLMM showed a main effects of enzyme treatment ($\chi^2 = 69$, $p_{FDR} < 0.0001$) and digestion time ($\chi^2 = 310$, $p_{FDR} < 0.0001$), as well as an interaction of treatment and time ($\chi^2 = 19.5$, $p_{FDR} = 0.022$).

From 10 minutes onwards, the slope of the grey value curves for boli with amylase was consistently lower than that for pepsin-treated boli and boli with no enzyme (Table 3). The greatest difference between amylase-treated and pepsin treated boli was found at $t = 30$ min. The slope of amylase-treated boli was 54% lower than that of pepsin-treated boli ($p < 0.0001$). At $t = 60$ min, the slope of amylase-treated boli was 47% of that of no enzyme boli. There was no difference in slope between no-enzyme and pepsin-treated boli (all $p \geq 0.18$).

Table 3 Pairwise comparisons for the treatments × time interaction on the slope of the grey value curves

Treatment comparison	Time (min)	Ratio[a]	95% CI	p
Amylase/no enzyme	0	1.01	0.69, 1.48	0.996
	10	0.53	0.37, 0.78	<0.001
	30	0.53	0.31, 0.67	<0.001
	60	0.47	0.32, 0.69	<0.0001
	90	0.50	0.34, 0.73	<0.0001
Amylase/pepsin	0	0.84	0.58, 1.23	0.53
	10	0.58	0.40, 0.84	0.002
	30	0.46	0.31, 0.67	<0.0001
	60	0.58	0.40, 0.84	0.002
	90	0.66	0.45, 0.97	0.028

[a] Estimated ratio of marginal mean slope of the grey value curves for amylase-treated boli to that of no enzyme boli or the pepsin-treated boli. Ratio and 95% CI are back-transformed from GLMM contrasts on the log scale.

The differences in slopes of grey value curves of ROIs with increasing depth may be attributed to water absorption and associated physical changes during digestion. As the SGF infiltrated and digestion progressed, the structure of amylase-treated boli became looser, with the wrapped air pockets and porous bread structure being filled by gastric fluid. This led to a more uniform internal texture which facilitated deeper ultrasound transmission and more echo signal at internal interfaces. In contrast, the no enzyme boli and the pepsin-treated boli did not expand rapidly and were not visibly degraded.

Overall, the looser structure, lower density, and rapidly dissolving air in amylase-treated boli can lead to deeper sound wave penetration, resulting in a slower decrease in grey value over imaging depth reflected by lower slope. These results suggest that slope of grey value curves can be an indicator of changes in boli properties during digestion, since it may reflect variations in signal intensity related to sound wave transmission.

3.2 Changes in bolus moisture content and density

Both bolus mean grey value and the image texture features of amylase treated boli differed from those of boli with pepsin and no enzyme. These differences are likely related to structural and physical changes associated with the starch hydrolysis.

To further investigate the underlying causes, we compared the density and moisture content of amylase boli before and after digestion (as shown in Fig. S5 in SI). Contrary to the possible interpretation mentioned above in section 3.1.1, *i.e.*, that variations in density will influence echogenicity, one-way ANOVA result showed that there were no apparent changes in density over time (p = 0.55). However, it must be noted that echogenicity is related to density changes on a microstructural level and not on a macro level. Furthermore, the lack of detectable changes in density may be partially attributed to methodological factors. The density of bread boli is close to that of water, and the drainage measurement used may be insensitive to small variations. Moreover, as digestion progressed, the peripheral regions of the boli tended to expand, where the density changed more significantly than in the core. However, when the boli were removed from the digestive solution, some water absorbed at the periphery was lost, so only the density of the denser core, which retained a similar density as that of undigested boli, could be measured. These factors may contribute to an overestimation of density.

Moisture content increased during digestion. A one-way ANOVA with time as the independent factor and moisture as the dependent factor showed a main effect of time ($F(4,10)$ = 6.31, p = 0.008). *Post-hoc* Tukey tests showed that moisture at 10 min (mean ± SD = 60.6 ± 3.09, p = 0.062) and 30 min (mean ± SD = 58.6 ± 1.61, p = 0.21) did not differ from 0 min (mean ± SD = 52.8 ± 2.60). Bolus moisture at 60 min (mean ± SD = 62.5 ± 4.67, p = 0.019) and 90 min (mean ± SD = 64.1 ± 2.32, p = 0.007) were higher than at 0 min. No other pairwise differences were found (all p > 0.24). The slight increase in moisture content may have contributed to deeper sound wave penetration and reduced scattering. An *ex vivo* study investigated the use of ultrasound to measure muscle dehydration, and found that when other tissue components including proteins and fat remained constant, ultrasound velocity increased with volumetric water loss.[31] As acoustic impedance is the product of density and sound speed, if bolus density remained stable or slightly decreased, and the sound speed decreased because of higher water content, acoustic impedance would decrease. This would allow sound waves to penetrate deeper and increase reflection, which expands the detectable bolus area on ultrasound images. Therefore, we speculate that the 5–10% increase in water content that we observed would be sufficient to produce differences in sound wave amplitudes. However, similar to what discussed for density measurements, moisture measurement may also have suffered from methodological limitations. The swollen outer bolus layers may indeed affect the accuracy of moisture measurements, because it is difficult to collect and measure precisely how much water was incorporated into the boli. As the fluid penetrates from the exterior to the interior, the periphery would have a higher water content than the core, which was confirmed by the dry and porous structures in the core of the boli even after 90 min digestion. However, when the boli were removed from the solution, water retained in those fully water-filled bread chunks tended to be lost, leading to an underestimation of water content. Examples are shown in Fig. S6 in SI.

3.3 Static *in vitro* starch and protein digestion in boli

Starch digestibility in the amylase treated boli increased progressively, from baseline to 10 minutes and from 30 to 60 minutes, reaching approximately 22%, and ended with a plateau (Fig. S7 in SI). While it is well-known that amylase becomes inactive at low pH, it can remain active for some time due to the buffering capacity of food, until the pH gradually drops to around 3.5.[32] Some studies show that, before being inactivated by the acidic gastric environment, 30–80% of starch can be hydrolysed, with up to half of it being broken down into oligosaccharides.[33,34] It should be noted that the degree of starch hydrolysis may be overestimated because the GOPOD assay includes a step to convert starch-derived intermediates into glucose. However, because this step was applied consistently across all time points, the trends and comparisons among digestion intervals remain valid.

In contrast, protein hydrolysis, as reflected by the release of amino acid groups, remained low throughout the whole digestion period and did not exceed 1%. This limited extent of protein digestion may be attributed to the fact that the majority of proteins in wheat flour are gluten proteins, which are mainly composed of gliadin and glutenin. Their high proline and glutamine content contribute to their resistance to gastric proteolysis.[35–37]

The digestion trends measured aligned with the ultrasound imaging results. The greater degree of expansion and structural breakdown represented by the slopes was correlated with the digestibility of starch (rho = −0.85, p_{FDR} < 0.0001) and protein (rho = −0.76, p_{FDR} < 0.01) (Fig. S8 in SI). In images of amylase-treated boli, *homogeneity* showed a significant positive correlation with starch digestibility (rho = 0.8, p_{FDR} < 0.0001), while *entropy* showed a significant negative correlation (rho = −0.81, p_{FDR} <0.0001). In pepsin-treated boli, moderate correlations were observed between protein hydrolysis and *homogeneity* (rho = 0.52, p_{FDR} = 0.048) and *entropy* (rho = −0.59, p_{FDR} = 0.024). These findings support the interpretation that ultrasound image features can reflect structural degradation associated with starch hydrolysis in bread boli. Although statistically significant correlations were found in the pepsin treatment

boli, the extremely low level of protein hydrolysis suggests that visual expansion does not necessarily correspond to biochemical breakdown in samples with low protein content. Bread was selected as a model food due to its relatively uniform structure, however our ultrasound imaging approach is not restricted to this substrate and may be used for a wide range of food matrices with varying compositions and structural properties. A clearer relationship between protein hydrolysis and image features may be observed in protein-rich foods.

A limitation of the present study relates to the segmentation of bolus regions on the ultrasound images. Although the wand tool in QuPath applies consistent parameter settings, the adjustment of the semi-automatic segmentation remains partly operator-dependent. The seed selection sensitivity was assessed on representative images, suggesting that seed selection had limited effect on area measurements and on solidity as a measure of shape. In images with clear contrast between bolus and background, segmentation was generally consistent. However, when the boundary became less distinct, the delineation became less precise which may introduce minor variability. This limitation is inherent to image-based ROI selection. Regarding the degree of hydrolysis, a limitation is that amylase and pepsin were measured in separate treatments rather than together. This was a practical compromise to preserve analytical clarity. By isolating each enzyme's effect, the observed structural and hydrolysis-related changes could be more directly attributed to a specific enzymatic mechanism. Moreover, the large volume of SGF, constrained by technical requirements associated with the pressure of the surrounding water and imaging setup, resulted in a low bolus-to-fluid ratio. Dilution of hydrolysis products may reduce detection sensitivity, particularly for protein digestion. Future work could optimize the system to better mimic normal physiology. In addition, the digestion chamber is compatible with MRI, which could further characterize bolus breakdown, bolus internal structure and fluid distribution during digestion to inform the interpretation of ultrasound measurements, representing a direction for future research.

4 Conclusion

In conclusion, this study designed and applied an *in vitro* model compatible with ultrasound imaging to investigate the structural breakdown of standardized bread boli during gastric digestion. In addition to demonstrating that ultrasonography can capture how enzymes affect the structural degradation during controlled gastric digestion, grey value analysis and image texture metrics such as homogeneity and entropy were used to characterize the imaged boli, showing their potential as non-invasive indicators of digestibility and physical transformation. This proof-of-principle study established a foundation for broader research on bolus breakdown of multiple boli across different food matrices, and future work could extend these methods to dynamic *in vitro* and *in vivo* digestion.

Author contributions

Xinhang Li: writing – original draft, writing – review & editing, conceptualization, methodology, investigation, formal analysis, data curation, visualization. Edoardo Capuano: writing – review & editing, supervision, project administration, conceptualization, methodology, validation, resources. Chris L. de Korte: writing – review & editing, supervision, conceptualization, methodology, validation. Paul A. M. Smeets: writing – review & editing, supervision, project administration, conceptualization, methodology, validation, resources.

Conflicts of interest

There are no conflicts to declare.

Data availability

The data supporting this article can be found on OSF, DOI: https://doi.org/10.17605/OSF.IO/FETMS. The SI includes: the experimental workflow, representative bolus segmentation under different image contrast conditions, procedures for bolus size estimation and size-constrained segmentation, texture analysis results for the constrained bolus area, measurements of density and moisture content, starch and protein digestibility, and correlation analyses between hydrolysis and image texture features. Supplementary information is available. See DOI: https://doi.org/10.1039/d5fo04784f.

Acknowledgements

The authors would like to thank Johan Belgraver of the AFSG Technical Development Studio for building the *in vitro* setup, Iman Ibrahim for the first pilot testing and Dr João Caldas Paulo for her help during data analysis. We also gratefully acknowledge the input of Eus Schrauwen (Vallei Medical, Ede, NL) and Eric de Groot, MD PhD (Imagelabonline & Cardiovascular, Diepenheim, NL). X. L. acknowledges financial supported by the China Scholarship Council (Grant No. 202309110023).

References

1 T. Bohn, F. Carriere, L. Day, A. Deglaire, L. Egger, D. Freitas, *et al.*, Correlation between in vitro and in vivo data on food digestion. What can we predict with static in vitro digestion models?, *Crit. Rev. Food Sci. Nutr.*, 2018, **58**(13), 2239–2261.

2 C. Shani-Levi, P. Alvito, A. Andrés, R. Assunção, R. Barberá, S. Blanquet-Diot, *et al.*, Extending in vitro digestion models to specific human populations: Perspectives, practical tools and bio-relevant information, *Trends Food Sci. Technol.*, 2017, **60**, 52–63.

3 A. Brodkorb, L. Egger, M. Alminger, P. Alvito, R. Assunção, S. Ballance, *et al.*, INFOGEST static in vitro simulation of gastrointestinal food digestion, *Nat. Protoc.*, 2019, **14**(4), 991–1014.
4 Y. Tan, H. Zhou and D. J. McClements, Application of static in vitro digestion models for assessing the bioaccessibility of hydrophobic bioactives: A review, *Trends Food Sci. Technol.*, 2022, **122**, 314–327, DOI: 10.1016/j.tifs.2022.02.028.
5 P. A. M. Smeets, R. Deng, E. J. M. Van Eijnatten and M. Mayar, Monitoring food digestion with magnetic resonance techniques, *Proc. Nutr. Soc.*, 2021, **80**(2), 148–158.
6 S. W. Smith and H. Lopez, A contrast-detail analysis of diagnostic ultrasound imaging, *Med. Phys.*, 1982, **9**(1), 4–12, DOI: 10.1118/1.595218.
7 G. Zhang, X. Huang, Y. Shui, C. Luo and L. Zhang, Ultrasound to guide the individual medical decision by evaluating the gastric contents and risk of aspiration: A literature review, *Asian J. Surg.*, 2020, **43**(12), 1142–1148.
8 J. Hlebowicz, J. M. Jönsson, S. Lindstedt, O. Björgell, G. Darwich and A. Lo, Effect of commercial rye whole-meal bread on postprandial blood glucose and gastric emptying in healthy subjects, *Nutr. J.*, 2009, **8**(1), 26.
9 W. Liu, W. Jin, P. J. Wilde, Y. Jin, Y. Pan and J. Han, Understanding the mechanism of high viscosity food delaying gastric emptying, *Food Funct.*, 2024, **15**(10), 5382–5396.
10 Y. Sakata, T. Yago, S. Mori, N. Seto, Y. Matsunaga, H. Nakamura, *et al.*, Time Courses of Gastric Volume and Content after Different Types of Casein Ingestion in Healthy Men: A Randomized Crossover Study, *J. Nutr.*, 2022, **152**(11), 2367–2375, DOI: 10.1093/jn/nxac158.
11 A. S. Giacomozzi, J. Benedito, A. Quiles, J. V. García-Pérez and M. E. Dalmau, Ultrasonic monitoring of softening in solid foods during in-vitro gastric digestion, *J. Food Eng.*, 2024, **374**, 112033.
12 A. Avila-Sierra, N. Decerle, M. Ramaioli and M. A. Peyron, Effect of salivary fluid characteristics on the physical features of in vitro bread bolus: from the absence of saliva to artificially simulated hypersalivation, *Food Res. Int.*, 2024, **175**, 113753.
13 J. Gao, S. Lin, X. Jin, Y. Wang, J. Ying, Z. Dong, *et al.*, In vitro digestion of bread: How is it influenced by the bolus characteristics?, *J. Texture Stud.*, 2019, **50**(3), 257–268.
14 P. Bankhead, M. B. Loughrey, J. A. Fernández, Y. Dombrowski, D. G. McArt, P. D. Dunne, *et al.*, QuPath: Open source software for digital pathology image analysis, *Sci. Rep.*, 2017, **7**(1), 1–7.
15 R. M. Haralick, I. Dinstein and K. Shanmugam, Textural Features for Image Classification, *IEEE Trans. Syst. Man. Cybern.*, 1973, **SMC-3**(6), 610–621.
16 P. Brynolfsson, D. Nilsson, T. Torheim, T. Asklund, C. T. Karlsson, J. Trygg, *et al.*, Haralick texture features from apparent diffusion coefficient (ADC) MRI images depend on imaging and pre-processing parameters, *Sci. Rep.*, 2017, **7**(1), 4041, DOI: 10.1038/s41598-017-04151-4.
17 D. Caruso, M. Zerunian, M. Ciolina, D. de Santis, M. Rengo, M. H. Soomro, *et al.*, Haralick's texture features for the prediction of response to therapy in colorectal cancer: a preliminary study, *Radiol. Med.*, 2018, **123**(3), 161–167.
18 I. R. Mansour and R. M. Thomson, Haralick texture feature analysis for characterization of specific energy and absorbed dose distributions across cellular to patient length scales, *Phys. Med. Biol.*, 2023, **68**(7), 075006.
19 A. Wibmer, H. Hricak, T. Gondo, K. Matsumoto, H. Veeraraghavan, D. Fehr, *et al.*, Haralick texture analysis of prostate MRI: utility for differentiating non-cancerous prostate from prostate cancer and differentiating prostate cancers with different Gleason scores, *Eur. Radiol.*, 2015, **25**(10), 2840–2850.
20 J. Schindelin, I. Arganda-Carreras, E. Frise, V. Kaynig, M. Longair, T. Pietzsch, *et al.*, Fiji: An open-source platform for biological-image analysis, *Nat. Methods*, 2012, **9**(7), 676–682.
21 F. Kong and R. P. Singh, Modes of disintegration of solid foods in simulated gastric environment, *Food Biophys.*, 2009, **4**(3), 180–190.
22 D. Freitas, L. G. Gómez-Mascaraque and A. Brodkorb, Digestion of protein and toxic gluten peptides in wheat bread, pasta and cereal and the effect of a supplemental enzyme mix, *Front. Nutr.*, 2022, **9**, 986272.
23 M. Byra, L. Wan, J. H. Wong, J. Du, S. B. Shah, M. P. Andre, *et al.*, Quantitative Ultrasound and B-Mode Image Texture Features Correlate with Collagen and Myelin Content in Human Ulnar Nerve Fascicles, *Ultrasound Med. Biol.*, 2019, **45**(7), 1830–1840.
24 E. J. M. van Eijnatten, G. Camps, M. Guerville, V. Fogliano, K. Hettinga and P. A. M. Smeets, Milk coagulation and gastric emptying in women experiencing gastrointestinal symptoms after ingestion of cow's milk, *Neurogastroenterol. Motil.*, 2023, 1–11.
25 L. Marciani, S. E. Pritchard, C. Hellier-Woods, C. Costigan, C. L. Hoad, P. A. Gowland, *et al.*, Delayed gastric emptying and reduced postprandial small bowel water content of equicaloric whole meal bread versus rice meals in healthy subjects: novel MRI insights, *Eur. J. Clin. Nutr.*, 2013, **67**(7), 754–758.
26 J. Nadia, J. E. Bronlund, H. Singh, R. P. Singh and G. M. Bornhorst, Contribution of the proximal and distal gastric phases to the breakdown of cooked starch-rich solid foods during static in vitro gastric digestion, *Food Res. Int.*, 2022, **157**, 111270; https://www.sciencedirect.com/science/article/pii/S0963996922003271.
27 D. Mitrea, M. Socaciu, R. Badea and A. Golea, Texture based characterization and automatic diagnosis of the abdominal tumors from ultrasound images using third order GLCM features. In: 2011 4th International Congress on Image and Signal Processing, 2011, pp. 1558–1562.
28 L. R. Sultan, S. S. B. Venkatakrishna, S. A. Anupindi, S. Andronikou, M. R. Acord, H. J. Otero, *et al.*, ChatGPT-4–Driven Liver Ultrasound Radiomics Analysis: Diagnostic Value and Drawbacks in a Comparative Study, *JMIR AI*, 2025, **4**, e68144; https://ai.jmir.org/2025/1/e68144.

29 R. Guo, H. Zhong, F. Xing, F. Lu, Z. Qu, R. Tong, *et al.*, Magnetic susceptibility and R2*-based texture analysis for evaluating liver fibrosis in chronic liver disease, *Eur. J. Radiol.*, 2023, **169**, 111155, DOI: 10.1016/j.ejrad.2023.111155.

30 E. J. M. van Eijnatten, G. Camps, W. Rombouts, L. Pellis and P. A. M. Smeets, Gastric Digestion and Changes in Serum Amino Acid Concentrations after Consumption of Casein from Cow and Goat Milk: A Randomized Crossover Trial in Healthy Males, *J. Nutr.*, 2025, **155**(10), 3374–3383.

31 A. Sarvazyan, A. Tatarinov and N. Sarvazyan, Ultrasonic assessment of tissue hydration status, *Ultrasonics*, 2005, **43**(8), 661–671; https://www.sciencedirect.com/science/article/pii/S0041624X05000120.

32 J. L. Rosenblum, C. L. Irwin and D. H. Alpers, Starch and glucose oligosaccharides protect salivary-type amylase activity at acid pH, *Am. J. Physiol.: Gastrointest. Liver Physiol.*, 1988, **254**(5), G775–G780.

33 D. Freitas and S. Le Feunteun, Oro-gastro-intestinal digestion of starch in white bread, wheat-based and gluten-free pasta: Unveiling the contribution of human salivary α-amylase, *Food Chem.*, 2019, **274**, 566–573, DOI: 10.1016/j.foodchem.2018.09.025.

34 D. Freitas, S. Le Feunteun, M. Panouillé and I. Souchon, The important role of salivary α-amylase in the gastric digestion of wheat bread starch, *Food Funct.*, 2018, **9**(1), 200–208.

35 D. Stepniak, L. Spaenij-Dekking, C. Mitea, M. Moester, A. De Ru, R. Baak-Pablo, *et al.*, Highly efficient gluten degradation with a newly identified prolyl endoprotease: Implications for celiac disease, *Am. J. Physiol.: Gastrointest. Liver Physiol.*, 2006, **291**(4), 621–629.

36 F. Cristofori, R. Francavilla, D. Capobianco, V. N. Dargenio, S. Filardo and P. Mastromarino, Bacterial-Based Strategies to Hydrolyze Gluten Peptides and Protect Intestinal Mucosa, *Front. Immunol.*, 2020, **11**, 567801.

37 P. R. Shewry and N. G. Halford, Cereal seed storage proteins: structures, properties and role in grain utilization, *J. Exp. Bot.*, 2002, **53**(370), 947–958, DOI: 10.1093/jexbot/53.370.947.

